arXiv:1701.04897v2 [cond-mat.mtrl-sci] 4 Feb 2017

Grain Boundary Resistance in Copper Interconnects from an Atomistic Model to a Neural Network

Daniel Valencia* and Evan Wilson

Birck Nanotechnology Center, Network for Computational Technology, Purdue University, West Lafayette, 47907, USA

Zhengping Jiang

Samsung Semiconductor Inc, San Jose CA, 95134, USA

Gustavo A. Valencia-Zapata, Gerhard Klimeck, and Michael Povolotskyi

Birck Nanotechnology Center, Network for Computational Technology, Purdue University, West Lafayette, 47907, USA

Abstract

Orientation effects on the resistivity of copper grain boundaries are studied systematically with two different atomistic tight binding methods. A methodology is developed to model the resistivity of grain boundaries using the Embedded Atom Model, tight binding methods and non-equilibrum Green's functions (NEGF). The methodology is validated against first principles calculations for small, ultra-thin body grain boundaries ($< 5nm$) with 6.4% deviation in the resistivity. A statistical ensemble of 600 large, random structures with grains is studied. For structures with three grains, it is found that the distribution of resistivities is close to normal. Finally, a compact model for grain boundary resistivity is constructed based on a neural network.

* valencid@purdue.edu

I. INTRODUCTION

Due to the aggressive downscaling of logic devices, interconnects have reached the nanoscale, making quantum effects important. According to the roadmap provided by ITRS, interconnects are expected to reach sizes of 10 to 20 nm in the next decade [1]. Previous work by Graham et al. [2] demonstrates that surface scattering and grain boundary (GB) scattering play major roles in the resistivity of structures smaller than 50 nm. Earlier works based on semi-empirical parameters have described polycrystalline films and surface scattering [3, 4] for macroscopic systems, but unfortunately scaling factors limit the scope of their applications. The ultra-scaled interconnects suggested by the roadmap require better descriptions of orientation and confinement effects to correctly model scattering in wires. Recently, first-principles calculations have been used to describe the resistance of a single grain by making use of non-equilibrium Green's function with Density Functional Theory (DFT-NEGF) formalism [5]. The results demonstrate a strong correlation between resistivity and local structures, and show agreement with both experimental [6] and other theoretical work [7, 8]. However, the studied structures are limited to relatively small sizes containing single grain boundaries and less than a few hundred atoms because of the computational burden required to perform DFT-NEGF calculations.

In this work, two different atomistic tight-binding models are used to describe copper interconnects. Section II describes the main characteristics of the models and benchmarks tight binding parameters against first principles calculations for a copper FCC structure. Section III constructs single grain boundaries based on coincident site lattice (CSL) and validates their electronic properties against an *ab initio* method. Following the ITRS road map, Section IV describes grain boundaries of 30 nm length simulated with an atomistic method to study the effects of grain boundary orientation on the resistivity. Section V proposes a statistical neural network approach which generalizes the results obtained from the atomistic methods to any configuration of grain boundary system with a total length of 30 nm.

II. DESCRIPTION OF TIGHT BINDING MODELS

The two tight binding methods used in this study are an environmental orthogonal tight binding model (TB) [9] and a non-orthogonal tight binding method based on the Extended Hückel (EH) model [10]. The TB model has an orthogonal basis with an interaction radius up to the second nearest neighbor (2NN). However, it requires a large number of parameters to include strain effects (48 parameters for copper). In comparison, the EH model has a non-orthogonal basis with a larger interaction radius up the third nearest neighbor (3NN). It requires a smaller number of parameters than the TB method (11 parameters for copper).

Existing parameters for the TB model [9] fail when used in highly distorted atomic systems such as GB. Due to the exponential dependence of the inter-atomic coupling on the bond length, the inter-atomic matrix elements with a 5% bond length distortion generate unphysical results. The problem is solved by obtaining a new parametrization with additional constraints on the inter-atomic coupling. This new parameter set is summarized in TABLE VI A in Appendix A.

The parameters for the EH model are taken from literature [11]. Both EH parameters and the new TB parameters show a good match for the Cu unit cell when compared against an *ab initio* method. The *ab initio* result, used as a reference, is obtained by density functional method with a Perdew-Burke-Ernzerhof version of the generalized gradient approximation (GGA PBE) exchange- correlation functional [12]. An energy cutoff of 150 Ry is used and the Brillouin zone is sampled with a 10×10×10 mesh. An FCC copper lattice with a lattice constant of 0.361 nm, as reported experimentally [13], is considered.

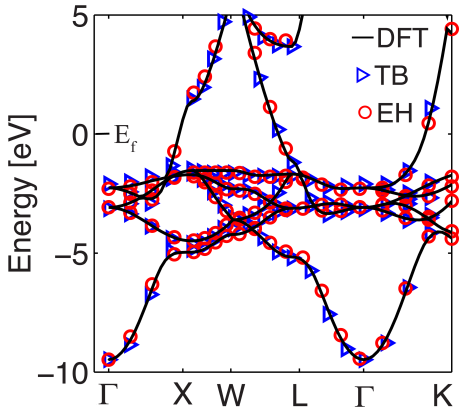

FIG. 1. Band structure for copper unit cell obtained by TB, EH and DFT methods. E_f indicates the Fermi energy.

III. COINCIDENT SITE LATTICE GRAIN BOUNDARIES

To validate the tight binding models, the effects of GB scattering were studied for a single coincident site lattice grain boundary. The simplest GB configurations are obtained by a rotation of one of the grains until its lattice vector becomes coincident with the vector of the unrotated lattice [14] as shown in Fig. 2. A fairly small number of atoms (< 400) is required to construct these systems, which allows tight binding models to be benchmarked against a first principles calculation as implemented in the ATK package [12].

CSLs are labeled by ΣN, where N corresponds to the ratio of the CSL unit cell size to the standard unit cell size. In this work, the CSL GB are generated with GBSTUDIO [15] and relaxed using an *ab initio* method. The relaxation is carried out with GGA PBE exchange-correlation functional. A Double Zeta polarized basis set is used for Copper atoms with an energy cutoff is 150 Ry and the Brillouin zone sampled with a 4×4×1 mesh, until all atomic forces on each ion are less than 10^{-5} eV/Å. Once the ionic relaxation is completed, the transmission spectrum for CSL structures is calculated by the recursive Green function method [16] implemented in NEMO5 [17] in an energy range between -2 and 2 eV around the Fermi level with a Brillouin zone sampled with a 30×30×1 mesh.

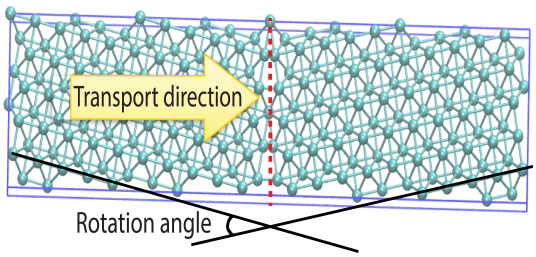

FIG. 2. Coincident site lattice GB are obtained by generating a superposition of two periodic lattices. One of the lattices was rotated with respect to the other, generating coincident points between the lattices for each rotation angle.

The integrated transmission spectra on the k space is obtained by the tight binding methods is compared against the spectrum obtained by the *ab initio* method with a similar basis set, energy cutoff and Brillouin mesh as is used in the ionic relaxation. The results in Fig. 3 show that the EH method captures the main features of DFT not only at the Fermi energy (E_f), but also over a large energy window. On other hand, while the transmission spectrum calculated by TB also shows reasonable agreement with DFT around the Fermi window, it fails to describe the *ab initio* transmission spectrum for energies away from the E_f.

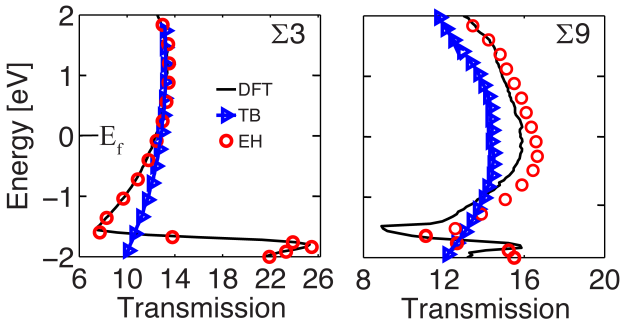

FIG. 3. Transmission spectra $T(E)$ for two different CSL ($\Sigma 3$ and $\Sigma 9$) show that EH captures the main features of DFT.

Subsequently, the resistance for the CSL GB is obtained based on the Landauer formalism assuming a low bias condition [18] which required the transmission spectrum $T(E)$ obtained before as :

$$G = \frac{1}{R} = \frac{2\,e^2}{h} \int T(E_f, \mathbf{k})\, d^2k, \tag{1}$$

where G is the conductance, R is the resistance, e is the elementary charge, h is Planck's constant and $T(E_f, \mathbf{k})$ is the transmission for a particular wave vector $\mathbf{k}$ at the Fermi energy. The Fermi level in Figs. 1 and 3 are calculated at the leads of the device self consistently for DFT and non-self consistently for tight binding models. In this last case, the Fermi level is obtained by integrating over the DOS from $-\infty$ to E_f until this value become equal to the total number of electrons at a zero temperature approximation [19]. Following Ref. [5] the resistivities of the CSL grain boundaries are obtained by $\rho = R \times (W \times T)$, where W and T are the width and thickness of the total GB are shown in Fig. 4. The results show less than 6.4% difference in the resistivity between EH and DFT, and less than 9.1% between TB and DFT. Thus the atomistic methods (TB and EH), are able to describe copper interconnects with reasonable accuracy. These methods are chosen to study GB systems with 10^3 to 10^4 atoms because they require significantly fewer computer resources than the *ab initio* calculations [19].

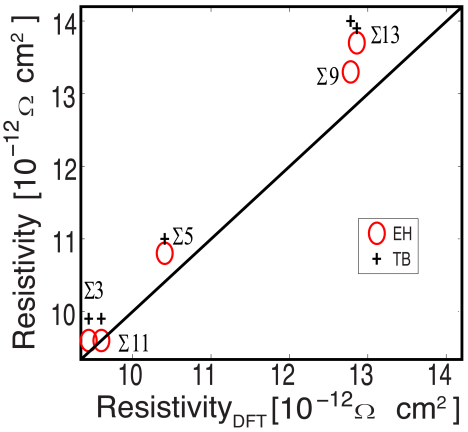

FIG. 4. Resistivities for different CSLs, labeled by ΣN, calculated by TB and EH and compared with the DFT method.

Only non *ab initio* methods are capable of relaxing structures of this size ($\gg 10^3$ atoms). In this study a semi-classical Embedded Atom Model (EAM) potential [20] implemented in LAMMPS [21] and benchmarked against first principles calculations. The accuracy of this approach is determined by comparing the total energy and final atomic positions for CSL GBs obtained by *ab initio* and EAM methods. The relaxation generated by *ab initio* is carried out with the plane wave DFT package (VASP) [22] and a PBE GGA exchange-correlation functional. The plane wave energy cutoff is 500 eV and the Brillouin zone is

sampled with a 4×4×1 mesh, until all atomic forces on each ion are less than 10^{-5} eV/Å. The total energy comparison is tabulated in TABLE I where E_{DFT} and E_{EAM} correspond to the total energy of the structure relaxed by first principles and semi-classical potential, respectively.

CSL GB	$E_{DFT}[eV]$	$E_{EAM} - E_{DFT}[eV]$	$(E_{EAM} - E_{DFT})/N_{atoms}$ $[eV]$
Σ5	-434.75	1.15	9.58×10^{-3}
Σ9	-1032.64	0.11	3.82×10^{-4}
Σ11	-1301.06	0.07	1.98×10^{-4}
Σ13	-765.26	0.04	2.41×10^{-3}

TABLE I. Total energy for different CSL structures, labeled by ΣN, calculated by the DFT method. E_{DFT} is total energy of structured relaxed by DFT method, E_{EAM} is the total energy of structure relaxed EAM method.

In order to observe the difference in the atoms' positions between a CSL GB relaxed with the EAM potential and DFT, the relaxed structures are shifted to have the same center of mass. Then, positions of corresponding atoms in both simulations are compared. The corresponding atoms are those that are closest in position as shown in Fig. 5. The median difference in the atoms' positions is less that 1 Å for all single CSL GBs.

Based on the results shown in TABLE I, the relaxation carried out by EAM potential shows a difference less than 1.1 eV in the DFT total energy (9.6×10^{-3} eV per atom). These results indicate that the EAM potential calculation is an acceptable method to relax the GB due to both the lower resource requirement and the reasonable difference in structure when compared with a structure relaxed with first principles calculations.

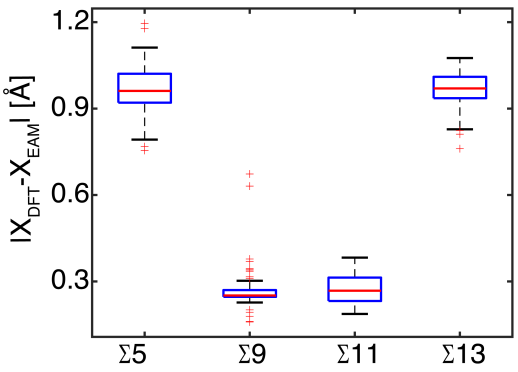

FIG. 5. Difference in atomic position for different single GBs relaxed with DFT and EAM.

IV. LARGE GRAIN BOUNDARIES

Based on the prediction of the ITRS roadmap that interconnects will reach sizes of 10 to 30 nm in the coming years [1], large GB of 30 nm length have been constructed starting with a homogeneous [110] oriented structure which has the highest conductance [9]. Two different types of GBs are generated by Voronoi diagrams [23] based on the rotation direction shown as "Tilt" and "Twist" GBs in Fig. 6 a) and b), respectively.

The "Tilt" GB are formed by three grains with thickness (T), width (W) and length (L) equal to 0.5 nm, 3 nm and 10 nm, respectively as shown in Fig. 6 a). Also included is a periodic boundary condition in the [001] direction with a GB generated by a rotation with respect to an axis parallel to the boundary by an angle θ between 0 and $\pi/2$.

The "Twist" GBs are also constructed with three grains where $T = W = 3$ nm and $L = 10$ nm and a periodic boundary condition is applied in the [001] direction. The middle grain is rotated perpendicular to the transport direction by an angle θ between 0 and $\pi/2$ as shown in Fig. 6 b).

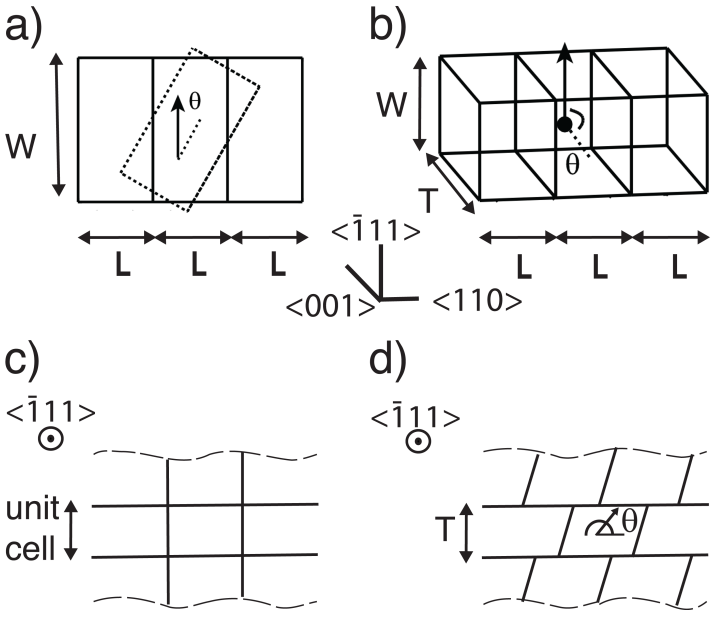

FIG. 6. GB classification: a) "Tilt" GB are generated by a rotation in the [001] plane b) "Twist" GB generated by a rotation in the [1̄01] plane. c) and d) figures represent the top view of "Tilt" and "Twist" GBs configuration

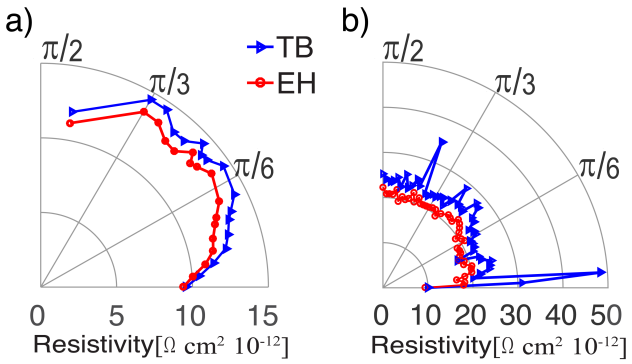

FIG. 7. a) "Tilt" and b) "Twist" GB resistivity calculated by TB and EH method.

The resistivity results for "Tilt" and "Twist" GBs are plotted in Fig. 7. Resistivity increases with the increase of angle in both systems, until the angle reaches $\pi/6$, and then becomes almost constant, although the "Tilt" GB shows a reduction after $\pi/3$. The resistivity dependence for "Twist" GBs is more spiky than for "Tilt" GBs, because "Twist" structure has more points per unit area, where the grain boundaries intersect (see Figs. 6c, d), which leads to higher number of dislocations. Differences between TB and EH, especially

pronounced for "Twist" GBs, are due to the fact that the TB model does not correctly describes strained systems, where the atoms are coupled by distances much smaller than the bulk bond length. In particular, for the "Twist" system with rotation angles, such as 6, 8 and 70 degrees, there are many atoms with small distance between nearest neighbors, that results in unphysical peaks in the resistivity dependence (see Fig. 7b) when it is calculated by TB method.

In order to understand and create a compact model to predict how resistivity changes as a result of GB orientation, a sample set of 600 configurations are generated. Each GB is constructed with three grains and each of them rotated with an angle (α, β, γ) between 0 to 180 degrees parallel to the GB boundary. The dimensions of the GB are similar to those used for "Tilt" GB with thickness, width and length equal to 0.5 nm, 3 nm and 10 nm, respectively as shown in Fig. 8. Periodic boundary condition in the [001] direction is imposed.

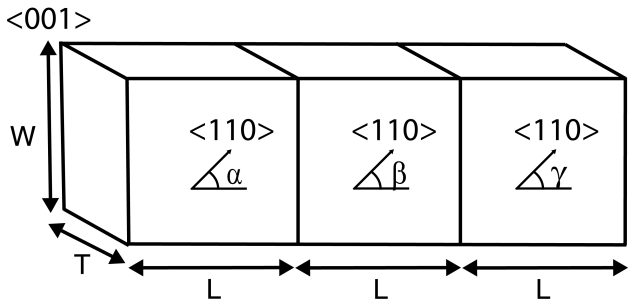

FIG. 8. GB configuration constructed with three grains, each one generated by rotating the lattice through angles α, β, γ, respectively, around the $< 001 >$ axis.

The resistivity for these samples is calculated with the EH method because this method is more reliable over angle rotations than the TB method. Making use of the results obtained for these samples, a boxplot for a constant angle β is plotted in Fig. 9 which shows a symmetry in the resistivity between 0 to 90 degrees and 90 to 180 degrees. This observation is confirmed by a statistic nonparametric Kolmogorov-Smirnov test [24] which compares the distribution function for the group of samples between 0 to 90 degrees against those between 90 to 180 degrees and finds that both groups of samples are drawn from an equivalent, continuous distribution. A p-value of 0.16 is obtained for the Kolmogorov-Smirnov test, confirming that there is no difference between the resistivity distributions for both cases with a confidence of 95%. The symmetry in the resistivity is due to the fact that the crystal symmetry of copper is not totally disrupted by the structural relaxation. The probability distribution for the three different angles (α, β and γ) between 90 to 180 degrees is plotted in Fig. 10.

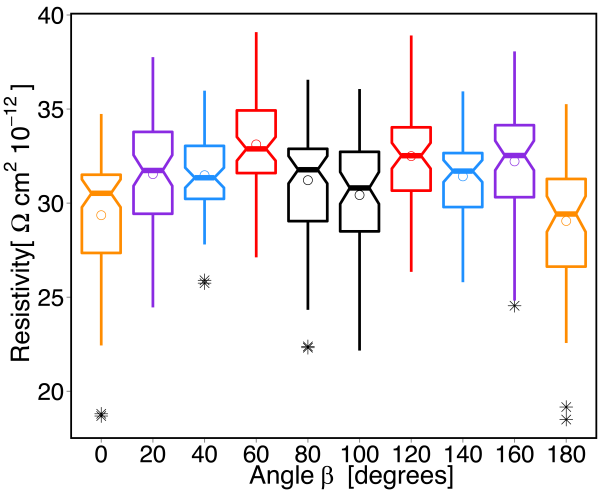

FIG. 9. Resistivity distributions for angle β. The boxplots represent the resistance distribution, while those marked with a star represent outliers.

Per the Shapiro-Wilk test [24] with a p value of 0.15 and a 95% confidence, the resistivity distribution follows a normal distribution with a mean and standard deviation equal to 31.7 $\times 10^{-12}\,\Omega\,cm^2$ and 2.8 $\times 10^{-12}\,\Omega\,cm^2$. The Q-Q plot in Fig. 10 b) shows that normality is likely a good approximation for the resistivity distribution, although the left and right tails do not follow a normal distribution. In order to describe the resistivity for any GB under a rotation (α, β and γ), a neural network model is proposed to parametrize the resistance. This compact model will describe the orientation effects on GB with the accuracy of an atomistic approximation and reduce the computational burden.

V. GB MODELED BY A NEURAL NETWORK

Atomistic models based on a tight binding approach can describe the effects of the GB orientation on resistivity with same accuracy as DFT methods, but with a much lower computational burden. However, atomistic models such as EH and TB are still not as fast as semi-empirical models when calculating the resistivity for GB with lengths greater than 30 nm [3, 4]. Therefore a compact model based on a Neural Network (NN) [25] algorithm is introduced. NN models have been widely used to model complex problems; in the TB approach NN algorithms have been used to describe potential minimization [26] and materials parametrization [27].

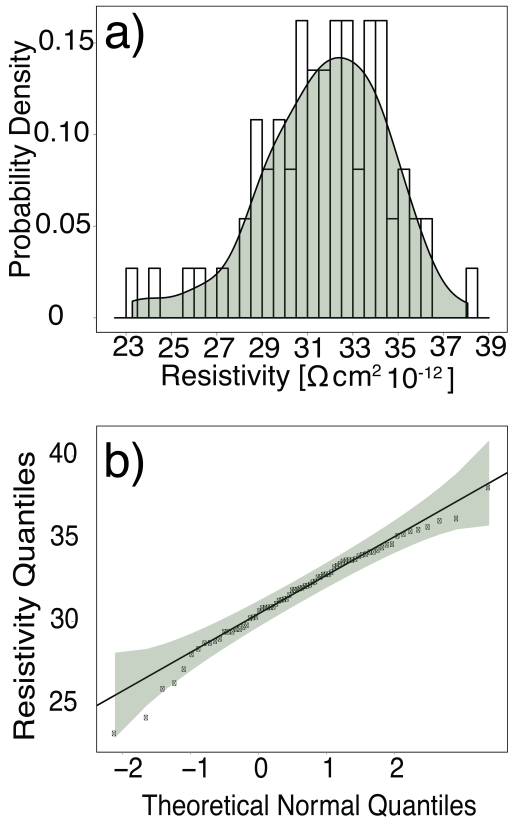

FIG. 10. a) Probability distribution for a GB system rotated over three different angles α, β and γ between 90 and 180 degrees, the shaded area represents the best approximated normal distribution for the 600 samples b) Q-Q plot which confirms the normal distribution.

In this work a multilayer neuronal network (MLN) is applied with a back-propagation algorithm [25] to quickly obtain the resistivity of the GB. The inputs of this model are the orientation angles α, β and γ and the output is the resistivity of the GB $\rho(\alpha, \beta, \gamma)$. The MLN model is trained with 80% of the 600 samples and validated with the remaining 20%.

The neural network shown in Fig. 11 is achieved after testing different types of neural networks and varying the number of hidden layers. The final system is formed by an input layer, three hidden layers, and one output layer. The input layer $\boldsymbol{p}= (\alpha, \beta, \gamma)$ is represented by a row vector of dimension 3×1. The hidden layer is composed of three inner layers i with 10, 6, and 3 neurons, respectively; the weight $\boldsymbol{W}^i$ and bias $\boldsymbol{b}^i$ vectors for a given layer i are shown in Fig. 11.

The MLN is implemented in the statistical software R making use of the package Neuralnet [28]. The value of the parameters $\boldsymbol{W}^i$ and bias $\boldsymbol{b}^i$ are obtained by the gradient descent

method [29] which minimizes the mean square error of the output layer. In the NN, the functions $\boldsymbol{f}^i$ represent logistic functions employed at each layer, except for the last layer $\boldsymbol{f}^4$ to which is applied a linear function.

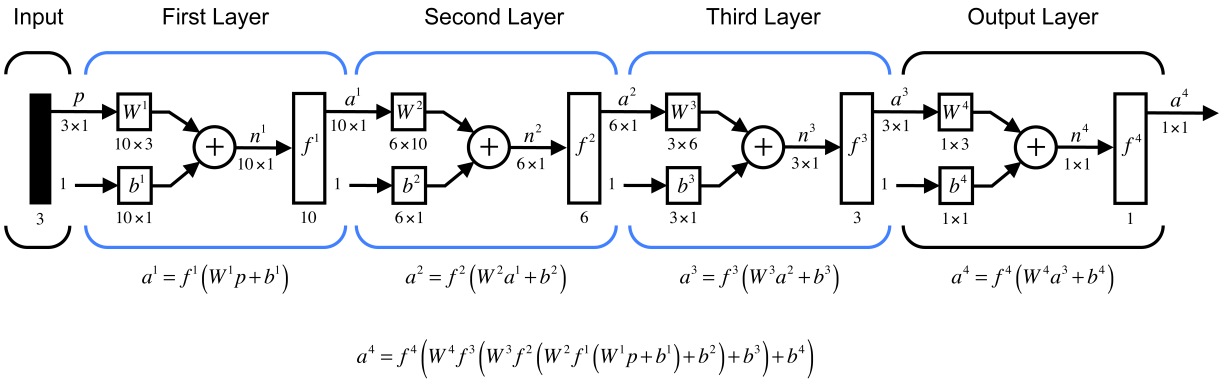
Input
First Layer
Second Layer
Third Layer
Output Layer
$a^1 = f^1\left(W^1 p + b^1\right)$
$a^2 = f^2\left(W^2 a^1 + b^2\right)$
$a^3 = f^3\left(W^3 a^2 + b^3\right)$
$a^4 = f^4\left(W^4 a^3 + b^4\right)$
$a^4 = f^4\left(W^4 f^3\left(W^3 f^2\left(W^2 f^1\left(W^1 p + b^1\right) + b^2\right) + b^3\right) + b^4\right)$

FIG. 11. Schematic representation for the Multi-Layer Neural Network used to describe grain boundary resistivity for copper interconnects with three grains. The values $\boldsymbol{W}^i$ and $\boldsymbol{b}^i$ correspond to the weights and bias parameters, $\boldsymbol{f}^i$ represents logistic functions except for the last layer $\boldsymbol{f}^4$ to which is applied a linear function and $\boldsymbol{a}^i$ corresponds to the output at each neuron i.

The mean square error (MSE) prediction for resistivity for this NN is $1.5\times10^{-12}\,\Omega\,cm^2$. The results obtained for the testing data of the MLN are plotted in Fig. 12; the model shows good agreement for low values of resistivity and larger variability for GB with a resistivity over the range 29.0 - $39.0\times10^{-12}\,\Omega\,cm^2$.

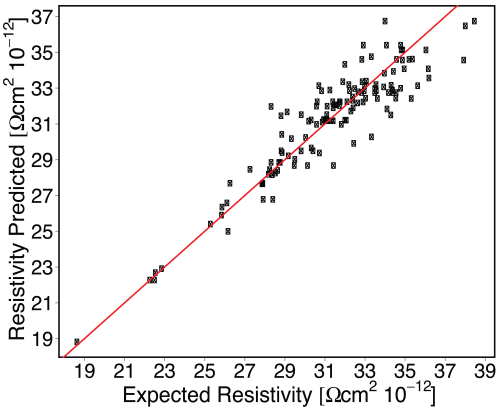

FIG. 12. Evaluation of the Multi-Layer Neural Network model for copper interconnects resistance.

VI. CONCLUSIONS

In summary, the effect of orientation on grain boundary resistance for copper interconnects is studied using two different atomistic tight binding methods (EH and TB). The transmission spectrum and resistivity calculated by these methods are benchmarked for coincident single GB (ΣN) against first principles calculations. These results show that the EH method captures the main features of DFT in the Fermi window between -2 to 2 eV. On other hand, the transmission spectrum calculated by TB also shows reasonable agreement with DFT around the Fermi window, but fails to describe the *ab initio* transmission spectrum for energies away from the Fermi energy. Since the computation requirements for tight binding methods are also much smaller than for first principle calculations, the EH method is an effective way to describe the resistivity of GB with lengths 30 nm and greater.

Orientation effects for "Tilt" and "Twist" GBs for copper interconnects of 30 nm length relaxed by a semi-classical EAM potential are also benchmarked against first principles. Rotations perpendicular to the transport direction have a larger effect on the resistivity of the GB than rotations parallel to the transport direction. Statistical analysis of GB resistivity shows that the inversion symmetry of the Cu is still manifested for the considered grain geometry.

Finally, a statistical model based on a neural network is introduced with an MSE lower than $1.5\times10^{-12}\,\Omega\,cm^2$, creating a compact model that describes the effect of orientation on "Tilt" GBs with 30 nm length. Future compact models could be generated that are trained using data from more sophisticated transport simulations that include effects as electron-phonon scattering.

ACKNOWLEDGMENTS

This work was supported by the FAME Center, one of six centres of STARnet, a Semiconductor Research Corporation program sponsored by MARCO and DARPA. Support by the US Department of Energys National Nuclear Security Administration under Grant No. DE-FC52-08NA28617 is acknowledged. The authors also acknowledge the staff and computing resources of both the Rosen Center for Advanced Computing (RCAC) at Purdue University and the Blue Waters sustained-petascale computing project, which is supported

by the National Science Foundation (award number ACI 1238993). Finally, the authors would like to thank Dr. Bozidar Novakovic and David Guzman for stimulating discussions about the topic.

A. Appendix

Parameters for bulk copper with the environmental tight binding method (TB) are obtained by direct fitting bulk band structure [9], but additional constraints on the inter-atomic coupling are included during the parametrization process.

Parameter Name	Value	Parameter Name	Value
VBO	3.6540	$I\_D\_D\_\Delta$	-0.08
E_S	-4.5236	$q\_D\_D\_\sigma$	4.8355
E_Px	-0.1458	$q\_D\_D\_\Pi$	4.7528
E_Py	-0.1458	$q\_D\_D\_\Delta$	4.2950
E_Pz	-0.1458	$I\_S\_S\_\sigma$	0.4
E_Dxy	-4.3034	$I\_S\_P\_\sigma$	0.4457
E_Dyz	-4.3034	$I\_S\_D\_\sigma$	-0.36819
E_Dxz	-4.3034	$I\_P\_P\_\sigma$	1.5605
E_Dz^2	-4.3034	$I\_P\_D\_\sigma$	-0.2532
$E\_Dx^2\_y^2$	-4.3034	$I\_P\_P\_\Pi$	-0.1348
$V\_S\_S\_\sigma$	-0.9588	$I\_P\_D\_\Pi$	0.0135
$V\_S\_P\_\sigma$	1.4063	$q\_S\_S\_\sigma$	2.20333
$V\_S\_D\_\sigma$	-0.1841	$q\_S\_P\_\sigma$	2.6554
$V\_P\_P\_\sigma$	1.4025	$q\_S\_D\_\sigma$	0.2495
$V\_P\_P\_\Pi$	-0.5730	$q\_P\_P\_\sigma$	1.5905
$V\_P\_D\_\sigma$	-0.4607	$q\_P\_P\_\Pi$	2.9059
$V\_P\_D\_\Pi$	0.3373	$q\_P\_D\_\sigma$	3.8124
$V\_D\_D\_\sigma$	-0.3709	$q\_P\_D\_\Pi$	3.9330
$V\_D\_D\_\Pi$	0.2760	$p\_S\_S\_\sigma$	1.3692
$V\_D\_D\_\Delta$	-0.0735	$p\_S\_P\_\sigma$	2.8794
$I\_D\_D\_\sigma$	-0.15	$p\_S\_D\_\sigma$	3.94296
$I\_D\_D\_\Pi$	-0.2498	$p\_P\_P\_\sigma$	5.5023
$p\_P\_P\_\Pi$	0.536231	$p\_P\_D\_\sigma$	-1
$p\_P\_D\_\Pi$	-1	$p\_D\_D\_\sigma$	-0.83723
$p\_D\_D\_\Pi$	0.66507	$p\_D\_D\_\Delta$	4.8475
R_0_inter	0.25526	R_0_intra	0.25526

TABLE II. TB parameters for Cu following the notation on ref [9]

[1] "International roadmap for semiconductors, http://public.itrs.net/reports.html," (2014).

[2] R. L. Graham, G. B. Alers, T. Mountsier, N. Shamma, S. Dhuey, S. Cabrini, R. H. Geiss, D. T. Read, and S. Peddeti, Applied Physics Letters **96**, 042116 (2010).

[3] K. Fuchs and N. F. Mott, Mathematical Proceedings of the Cambridge Philosophical Society **34**, 100 (1938).

[4] A. F. Mayadas, Applied Physics Letters **14**, 345 (1969).

[5] M. César, D. Liu, D. Gall, and H. Guo, Physical Review Applied **2**, 044007 (2014).

[6] T.-H. Kim, X.-G. Zhang, D. M. Nicholson, B. M. Evans, N. S. Kulkarni, B. Radhakrishnan, E. A. Kenik, and A.-P. Li, Nano letters **10**, 3096 (2010).

[7] B. Feldman, S. Park, M. Haverty, S. Shankar, and S. T. Dunham, physica status solidi (b) **247**, 1791 (2010).

[8] B. Zhou, Y. Xu, S. Wang, G. Zhou, and K. Xia, Solid State Communications **150**, 1422 (2010).

[9] G. Hegde, M. Povolotskyi, T. Kubis, T. Boykin, and G. Klimeck, Journal of Applied Physics **115**, 123703 (2014).

[10] R. Hoffmann, Reviews of Modern Physics **60**, 601 (1988).

[11] J. Cerdá and F. Soria, Physical Review B **61**, 7965 (2000).

[12] M. Brandbyge, J.-L. Mozos, P. Ordejón, J. Taylor, and K. Stokbro, Physical Review B **65**, 165401 (2002).

[13] M. E. Straumanis, L. S. Yu, and IUCr, Acta Crystallographica Section A **25**, 676 (1969).

[14] P. D. Bristowe and A. G. Crocker, Philosophical Magazine A **38**, 487 (1978).

[15] GBStudio, "https://staff.aist.go.jph.ogawa/GBstudio/indexE.html ,".

[16] R. Lake, G. Klimeck, R. C. Bowen, and D. Jovanovic, Journal of Applied Physics **81**, 7845 (1997).

[17] S. Steiger, M. Povolotskyi, H.-H. Park, T. Kubis, and G. Klimeck, "NEMO5: A Parallel Multiscale Nanoelectronics Modeling Tool," (2011).

[18] Supriyo Datta, *Electronic transport in mesoscopic systems* (Cambridge University Press, Cambridge, 1997).

[19] D. Valencia, E. Wilson, P. Sarangapani, G. A. Valencia-Zapata, G. Klimeck, M. Povolotskyi, and Z. Jiang, in *2016 International Conference on Simulation of Semiconductor Processes and Devices (SISPAD)* (IEEE, 2016) pp. 105–108.

[20] Y. Mishin, M. J. Mehl, D. A. Papaconstantopoulos, A. F. Voter, and J. D. Kress, Physical Review B **63**, 224106 (2001).

[21] S. Plimpton, Journal of Computational Physics **117**, 1 (1995).

[22] G. Kresse and J. Furthmüller, Computational Materials Science **6**, 15 (1996).

[23] C. H. Rycroft, G. S. Grest, J. W. Landry, and M. Z. Bazant, Physical Review E **74**, 021306 (2006).

[24] W. J. Conover, *Practical Nonparametric Statistics*, 3rd ed. (Wiley Publication, 1999).

[25] H. B. D. M. T. Hagan and M. H. Beale, *Neural network design* (PWS Publishing Company, 1996) p. 734.

[26] L. R. Marim, M. R. Lemes, and A. Dal Pino, Phys. Rev. A **67**, 033203 (2003).

[27] A. Bholoa, S. Kenny, and R. Smith, Nuclear Instruments and Methods in Physics Research Section B: Beam Interactions with Materials and Atoms **255**, 1 (2007).

[28] S. Fritsch, F. Guenther and M. Suling, *neuralnet: Training of Neural Networks* (R Foundation for Statistical Computing, 2008).

[29] S. Haykin, *Neural networks-A comprehensive foundation*, 2nd ed. (Prentice Hall, 1999).